Ruthenium polypyridyl squalene derivative: a novel self-assembling lipophilic probe for cellular imaging

Ruthenium polypyridyl squalene derivative: A novel self-assembling lipophilic probe for cellular imaging

Franco Dosio [a],∗, Barbara Stella [a], Annalisa Ferrero [a], Claudio Garino [b], Daniele Zonari [a], Silvia Arpicco [a], Luigi Cattel [a], Susanna Giordano [a], Roberto Gobetto [b]

[a] Dipartimento di Scienza e Tecnologia del Farmaco, Università degli Studi di Torino, via P. Giuria 9, 10125 Torino, Italy

[b] Dipartimento di Chimica, Università degli Studi di Torino, via P. Giuria 7, 10125 Torino, Italy

Abstract

Transition metal complexes provide a promising avenue for designing new therapeutic and diagnostic agents. In particular, ruthenium(II) polypyridyl complexes are useful for studying cellular uptake, due to their easy synthesis and unique photophysical properties. Dyes are frequently combined with material substrates to modulate their properties, enhance stability, reduce toxicity, and improve delivery. A novel Ru polypyridyl complex linked to a derivative of the natural lipid squalene (Ru-BIPPBI-hx-SQ) is described. Using the solvent displacement method, Ru-BIPPBI-hx-SQ easily self-assembles into nanosized aggregates in aqueous solution, as characterized by dynamic light scattering. The nanoassemblies exhibit long-lived and intense luminescence. Preliminary biological assessment showed them to be non-toxic; they are efficiently and rapidly transported across the cell membrane without requiring its permeabilization. Ru-labeled nanoassemblies are likely to be significant cellular-imaging tools, probing cellular events at very low concentrations. Moreover co-nanoassembly, with drug-derivatives based on squalenoylation technology, including gemcitabine and paclitaxel, has given interesting preliminary results.

∗ Corresponding author. Tel.: +39 0116707082; fax: +39 0112367697. E-mail address: franco.dosio@unito.it (F. Dosio).

1. Introduction

The nanotechnological approach to pharmacology is of considerable interest, in particular for designing drug-delivery tools; it is now leading to the appearance of new treatments with improved efficacy (Schroeder et al., 2012). Numerous nanomaterial-based therapeutics are now under development. Based on building blocks of different composition (polymeric, lipidic, metal based, carbon and biological) nanocompounds have been developed that can carry large amounts of drug,

releasing it under specific conditions, and with specific targeting moieties. A further advantage of using supramolecular structures is that imaging tools for diagnostic therapy can be delivered. The concept of chemically linking a terpenoid to a biologically active drug molecule to create a bioconjugate that can self aggregate in water, forming nanoassemblies, is a recent development. The concept was first applied for a hydrophilic compound, namely gemcitabine (Gem) (Couvreur et al., 2006), and later extended to a hydrophobic compound, namely paclitaxel (PTX) (Dosio et al., 2010). Other relevant anticancer drugs, namely cisplatin, doxorubicin, and siRNA bioconjugates, have also been developed (Raouane et al., 2011). Squalenoylation has been employed to embed superparamagnetic iron oxide nanoparticles, resulting in a new nanostructured tool for therapeutics and diagnosis (Arias et al., 2011). Cellular uptake is critical to evaluate therapeutic or diagnostic applications of nanoparticles and small molecules clearly. However, the chemical rules governing cellular uptake are not fully understood, and when it can be evaluated the techniques required are cumbersome. The most widely used probes in cellular imaging are fluorescent chromophores, typically based on polyaromatic organic compounds. Transition metal complexes are increasingly applied for biological applications, buttheir uptake properties have not been fully clarified (Boerner and Zaleski, 2005; Hart et al., 2006). Luminescent ruthenium complexes have been studied as oxygen sensors (Gerritsen et al., 1997) and as DNA intercalators (Zeglis and Barton, 2008). Other studies have addressed the use of Ru (II) complexes as anticancer agents (Lentz et al., 2009; Levina et al., 2009; Scolaro et al., 2005) and, more recently, as cellimaging probes. For this latter application, ruthenium complexes offer several advantages:low background emission, and other characteristic photophysical properties including a long-lived excited metal-to-ligand charge transfer state, and red-shifted emission. These characteristics combine to make them interesting candidates as molecular probes for cellular imaging using fluorescence microscopy.

Although Ru(II)–polypyridyl complexes have been widely studied, their use in practical applications as fluorophores for cellular imaging (Fernandez-Moreira et al., 2010) has remained limited. A drawback of some complexes is their inability to efficiently cross cell membranes, and various approaches have been attempted to improve cell penetration and specific intracellular distribution. A ruthenium complex conjugated to estradiol has been shown to be cellpenetrating,probablydue to the lipophilicity ofthe steroidmoiety (Lo et al., 2008). Other approaches involve conjugation with cell-penetrating peptides (Neugebauer et al., 2008), with biotin (Lo and Lee, 2007), and with Ru–oligonucleotide derivatives (Le Gac et al., 2009). Another unexplored field in which Ru(II) complexes might be of interest concerns their use as probes for nanoparticles. Initial applications in monitoring the uptake and intracellular fate of silica nanoparticles (Besic Gyenge et al., 2011) and of gold nanoparticles (Elmes et al., 2011) have

recently been reported. With the aim of expanding the squalenoylation platform to include novel cell-imaging probes, this study shows that conjugating a bulky complex [Ru(II) bis(2,2 -bipyridine)-{1-methyl-2- (4-methylpyridin-2-yl)-benzoimidazole}](PF6)$_2$ to squalene leads to the construction of stable nanoassemblies in water. Their photophysical properties, cell uptake, and distribution are examined. Preliminary evaluations of co-nanoassemblies comprising therapeutic and diagnostic tools are also reported.

2. Materials and methods

2.1. Materials

The reagents tert-butoxide, tert-butyl 6-bromohexylcarbamate, ammonium hexafluorophosphate, N-hydroxysuccinimide and all solvents were purchased from Sigma Aldrich (Milwaukee, WI), Ruthenium(III) chloride hydrate was purchased from Alfa Aesar (Karlsruhe, Germany) and used as received. 2-(4-Methylpyridin- 2-yl)-1H-benzoimidazole (Barni and Savarino, 1977), Dichlorobis (dipyridyl)Ruthenium (II) dihydrate [cis-[Ru(bpy)$_2$Cl$_2$]·2H$_2$O] (Sullivan et al., 1978) and N-hydroxysuccinimido diphenyl phosphate (SDPP) (Ogura et al., 1980) were prepared by known methods. 1,1 ,2-Trisnorsqualenoic acid was prepared as described in Ceruti et al. (1987) starting from squalene, via the intermediates squalene monobromohydrine and squalene 2,3-epoxide. The squalenoyl derivatives of Gem and PTX were prepared as described elsewhere (Couvreur et al., 2006; Dosio et al., 2010). In all studies involving fluorescence and in all cell tests, the compound [Ru(II) bis(2,2 -bipyridine){1-methyl-2-(4- methylpyridin-2-yl)-benzoimidazole}] (PF6)$_2$ (Ru-BPPBI), synthesized as described in Gobetto et al.(2006), was used for comparison. This compound was dissolved in dimethylsulfoxide before dilution in test solutions. The 1H NMR spectra were recorded using a NMR Bruker Avance 400 spectrometer (Bruker AXS Inc., Madison, WI). Spectroscopic signals were referenced to the residual solvent peak. The following abbreviations are used: s, singlet; d, doublet; t, triplet; m, multiplet. Elemental analyses were carried out by Redox Snc (Monza, Italy). Quasi-elastic light scattering (QELS) and zeta potential were measured using a 90 Plus Particle Size Analyzer (Brookhaven Instruments, Co., Holtsville, NY) photometer. UV-vis spectra were recorded using a Beckman 730 spectrophotometer with a temperature controller. Mass spectra were recorded with a Finnigan Mat TSQ700 and Waters Micromass ZQ (ESCI and APCI sources) (Waters Corp. Milford, MA). Photoemission spectra were acquired with a Horiba Jobin Yvon Fluorolog3 TCSPC spectrofluorimeter (Horiba Ltd., Minami-KuKyoto, Japan).

2.2. Synthesis

2.2.1. tert-Butyl 6-(2-(4-methylpyridin-2-yl)-1H-benzoimidazol- 1-yl)-hexylcarbamate Freshly sublimated potassium tert-butoxide (0.160 g, 1.40 mmol) was added to a solution of 2-(4-methylpyridin- 2-yl)-1H-benzoimidazole (0.250 g, 1.20 mmol) in anhydrous dimethylformamide/anhydrous diethyl ether (4 mL/8 mL), at room temperature in argon. After stirring for 15 min, a solution of tert-butyl 6-bromohexylcarbamate (1.14 g, 4.06 mmol) in dimethylformamide (2 mL) was added dropwise. After 8 h of heating at 60 ◦C, the mixture was cooled to room temperature, poured into water (10 mL) and extracted with chloroform (4 × 10 mL). The organic layers were dried with anhydrous sodium sulfate, evaporated under vacuum, and purified chromatographically over silica gel using diethyl ether as eluent. A yellowish solid was obtained with a yield of 75% (0.368 g). 1H NMR (400 MHz, [D4]-methanol): ı = 8.60 (d, 1H, 3J = 5.0 Hz), 8.03 (s, 1H), 7.72 (d, 1H, 3J = 7.9 Hz), 7.61 (d, 1H, 3J = 7.9 Hz), 7.39–7.30 (m, 3H), 4.77 (t, 2H, 3J = 7.3 Hz), 2.95 (t, 2H, 3J = 6.8 Hz), 2.50 (s, 3H), 1.83 (m, 2H, 3J = 6.8/7.3), 1.42 (s, 9H), 1.37 (m, 2H), 1.28 (m, 4H) ppm. m/z C24N4O2H32(ESI): 409 [M+H]+, 431 [M+Na]+.

2.2.2. [Ru(II) bis(2,2 -bipyridine) {6-[2-(4-methyl-pyridin-2-yl)- 1H-benzoimidazol-1-yl]-hexylamine}](PF6)^2 [Ru(bpy)2Cl2]·2H2O (0.300 g, 0.576 mmol) and tert-butyl 6-(2- (4-methylpyridin-2-yl)-1H-benzoimidazol-1-yl)-hexylcarbamate (0.280 g, 0.685 mmol) were dissolved in ethylene glycol (50 mL). The mixture was degassed with argon for 15 min and then refluxed for 6 h. After cooling to room temperature, water (20 mL) and an aqueous solution of NH4PF6 (1.0 g/10 mL) were added. The precipitate was then collected, washed with water (10 mL) and dried with diethyl ether. 0.420 g (0.415 mmol) of [Ru(II) bis(2,2-bipyridine) {6-[2-(4-methyl-pyridin-2-yl)-1Hbenzoimidazol-1-yl]-hexylamine}](PF6)$_2$ were obtained (yield 72%). 1H NMR (400 MHz, [D3]-acetonitrile): ı = 8.50 (m, 3H), 8.41 (d, 1H, 3J = 8.0 Hz), 8.19 (s, 1H), 8.10 (m, 1H), 8.08–8.03 (m, 2H), 7.96 (t, 1H, 3J = 7.9), 7.91 (d, 1H, 3J = 5.5), 7.80 (d, 1H, 3J = 5.4), 7.74 (m, 3H), 7.62 (d, 1H, 3J = 5.7), 7.46–7.30 (m, 5H), 7.25 (d, 1H, 3J = 5.2), 7.05 (t, 1 H, 3J = 8.0), 5.81 (d, 1H, 3J = 8.4), 4.80 (m, 2H), 2.58 (s, 3H), 2.10 (m, 1H), 1.99 (m, 2H), 1.40 (m, 6H) ppm.

2.2.3. Squalene- N-hydroxysuccinimide Ester 1,1 ,2-Trisnorsqualenoyl-N-hydroxysuccinimide ester (SQNHS) was synthesized using the SDPP reagent. Briefly, SDPP (1.5 equiv.) dissolved in anhydrous dichloromethane (10 mL) with triethylamine (4 equiv.) was added to a solution of 1,1 ,2-trisnorsqualenoic acid (300 mg, 0.749 mmol). The mixture was stirred for 3 h at room temperature and then concentrated under vacuum. The crude reaction mixture was dissolved in dichloromethane and extracted with brine, and further dried with magnesium sulfate. The reaction product did not require any further purification (yield 85%). ESI-MS calculated for SQ-NHS Found: 498.72 (M+H+).

2.2.4. Squalenoyl- [Ru(II) bis(2,2 -bipyridine) {6-[2-(4-methylpyridin-2-yl)-1H-benzoimidazol-1-yl]-hexylamine}](PF6)2 (Ru-BIPPBI-hx-SQ) [Ru(II) bis(2,2 -bipyridine) {6-[2-(4-methyl-pyridin-2-yl)-1Hbenzoimidazol-1-yl]-hexylamine}]$(PF6)_2$ (60 mg, 0.06 mmol) was dissolved in anhydrous dichloromethane (6 mL). An equivalent molar amount of SQ-NHS (30 mg) and triethylamine (10 μL, d = 0.76) were added under stirring and the reaction was allowed to continue for 4 h at 20 ◦C. After solvent removal, the crude mixture was purified by SiO_2 gel chromatography with linear gradients, using a dichloromethane/ethanol mixture as eluent, 98:2–90:10. Rf (dichloromethane/ethanol 9:1) = 0.4. A dark red oil resulted, with a yield of 75% (83 mg). C66H82F6N8OPRu m/z 1250.01 (M–PF6+H), peaks representative of Ru pattern. 1H NMR (400 MHz, CDCl3): ı = 8.52 (m, 3H), 8.41 (s, 1H, 3J = 8.0 Hz), 8.09–8.03 (m, 2H), 7.97 (t, 1H, 3J = 7.9), 7.90 (d, 1H, 3J = 5.4), 7.80 (d, 1H, 3J = 5.4), 7.74 (m, 3H), 7.61 (d, 1H, 3J = 5.5), 7.46–7.30 (m, 5H), 7.25 (d, 1H, 3J = 5.2), 7.05 (t, 1H, 3J = 7.8), 5.20 (m, 5H), 5.06 (s, 2H), 4.80 (m, 2H), 3.12 (t, 2H, 3J = 6.2), 2.43 (m, 5H), 2.31 (m, 4H), 2.00–1.89 (m, 18H), 1.69 (m, 2H), 1.61 (m, 20H), 1.38 (m, 6H) ppm.

2.2.5. Preparation of nanoassemblies

Nanoassemblies (NAs) were prepared as follows: the Ru-BPPBIhx-SQ conjugate was dissolved in acetone (4–8 mg/mL), after which the organic solution was added dropwise under rapid stirring into MilliQ grade water. Finally, the organic solvent was completely evaporated using Rotavapor®, leaving an aqueous suspension of NAs. In a typical nanoassembled preparation, the final concentration of Ru-BPPBI-hx-SQ was 2 mg/mL. Co-nanoprecipitation was achieved by dissolving precise amounts of squalenoyl derivatives of paclitaxel (PTX-SQ) or gemcitabine (Gem-SQ) (1 mg) with different molar proportions of Ru-BPPBI-hx-SQ (10%, 5%, 1%) in acetone, and following the above procedure.

2.3. Characterization

2.3.1. Size and zeta potential measurements

The average diameter and polydispersity index of the nanoassemblies were determined using quasi-elastic light scattering (QELS) at a fixed angle of 90 ◦C and at a temperature of 25 ◦C. The NA dispersions were diluted (10% or 20%) with MilliQ water before analysis. Each value reported is the average of ten measurements. To determine the electrophoretic mobility, the NA samples were diluted with 0.1 mM KCl and placed in the electrophoretic cell, where an electric field of 15.24V/cm was established. Each sample was analyzed in triplicate. Zeta potential values were calculated using the Smolochowski equation. The stability of NAs was assessed by repeating size

measurements of Ru-BPPBI-hx-SQ or of co-nanoassemblies up to 15 days after storage at 5 ◦C in the dark.

2.3.2. Photophysical characterization

Electronic absorption and photoemission spectra were recorded at room temperature in acetonitrile solution (Ru-BPPBI-hxSQ, [Ru(II) bis(2,2 -bipyridine) {6-[2-(4-methyl-pyridin-2-yl)-1Hbenzoimidazol-1-yl]-hexylamine}](PF6)$_2$, and Ru-BPPBI) or in aqueous solution (Ru-BPPBI-hx-SQ nanoassembly). Photoemission spectra were recorded in both degassed and air-saturated solutions. Photoemission spectra were acquired with a Horiba Jobin Yvon Fluorolog3 TCSPC spectrofluorimeter equipped with a 450W Xenon lamp and a Hamamatsu R928 photomultiplier. The spectral response was corrected for the spectral sensitivity of the photomultiplier. Luminescence quantum yields (ϕ) were determined using [Ru(bpy)^3]Cl$_2$ as standard (ϕ = 0.062) (Juris et al., 1988). The refractive index was corrected to account for the specific solvent used Luminescence lifetimes were determined by time-correlated single-photon counting (TCSPC). Excitation was with nanosecond pulses of 455 nm light (repetition rate 100 kHz) generated by a NanoLED pulsed diode. Emission data were collected using a spectral bandwidth of 5 nm at 90 ◦C to a TBX-4 detector. Data were collected into 1024 channels, to 10,000 counts in the peak channel. Emission decay data were analyzed using the software package DAS6 (TCSPC Decay Analysis Software).

2.3.3. Cell tests

Cell cultures: human breast-cancer cells (MCF-7, ATCC HTB-22) and human colorectal-adenocarcinoma cells (HT-29, ATCC HTB-38) were cultured in DMEM and RPMI, respectively, both supplemented with 10% foetal bovine serum (Invitrogen), and 1% antibiotics (containing penicillin and streptomycin, Invitrogen). The medium was changed every other day, and the culture was incubated at 37 ◦C in a humidified atmosphere containing 5% CO2. The liquid overlay technique was used to generate multicellular spheroids (Wartenberg and Acker, 1995). Briefly, cell monolayers of HT-29 were trypsinized and seeded on agarose-coated 10 cm Petri dishes at 1 × 10^5 cells/mL, in an incubator (37 ◦C, 5% CO2). A proportion of the cell-culture medium was changed daily. After 4 days of liquid overlay, the spheroids were stable in form; they reached the desired diameter of 70–100 m two days later. Selected multicellular spheroids were transferred to 35-mm Petri dishes in 2 mL of medium, and exposed to Ru-BPPBI-hx-SQ NA or to Ru-BPPBI (final concentration 50 μM) for 2 h, then washed three times in RPMI; fluorescence intensity was then measured using a confocal laser scanning microscopy technique, as described below.

2.3.4. Inductively coupled plasma mass spectrometric (ICPMS) detection of Ru

The MCF-7 cell line was grown to ~30% confluence in 75 cm^2 flasks, and incubated with 50 μM of either Ru-BPPBI or Ru-BPPBIhx-SQ for 1 h at 37 ◦C in serum-free medium. Cells were rinsed with RPMI, detached with trypsin, and counted. Aliquots of 3–4 million cells were isolated by centrifugation and digested with 1 mL of concentrated nitric acid (65%) for 1.5 h at 60 ◦C. The solution was diluted with 10 mL double-distilled water. The 102Ru content was measured using a Thermo Electron Corporation ELEMENT2 Inductively Coupled Plasma-Sector Field Mass Spectrometer (Thermo Fisher Sci., Waltham, MA, USA) by comparison with a standard curve of [Ru(bpy)3]Cl2 . 6 H2O (range 1–70 ppb). Data are reported as means plus standard deviation (n = 3).

2.3.5. Cytotoxicity assay

Cytotoxicity was assayed on MCF7 and HT-29 carcinoma cell lines, incubating the cells with different concentrations of NAs or Ru compounds for 72 h (37 ◦C, 5% CO2). The supernatant was removed, and the cells were washed and incubated for 16 h with 200 mL of medium containing 31 mCi of L-[4,5- ^{3}H]leucine (58 Ci/mmole) (Amersham). The cells were removed from the plates using Nonidet P-40 (1‰) and the incorporated radioactivity measured in a LS-5000TD beta-counter (Beckman). Results are expressed as percentage L-[4,5-3H]leucine incorporation versus controls; background values were subtracted. The experiment was repeated three times, in triplicate, for each concentration of the compounds.

2.3.6. Confocal laser scanning microscope studies

HT-29 and MCF-7 cell lines (about 0.3 × 10^6 cells) were seeded onto sterile glass two-well chamber slides 4.2 cm2 Lab-TekTM (Nunc Thermo Fisher Sci.) and cultured overnight (to about 70% confluence) prior to the experiments. Cells were washed twice with fetal-bovine-serum-free RPMI, and incubated for 2 h at 37 ◦C, 5% CO2, with either Ru-BPPBI-hx-SQ NA or Ru-BPPBI, diluted to 50 μM. After 2 h, cells were incubated with 200 μL of 4 ,6- diamidino-2-phenylindole (DAPI) (1 μg/mL in a free-serum RPMI; ex = 365 nm–em = 454 nm) for 30 min at 37 ◦C. Cells were then washed with PBS (2 × 2 mL) and fixed at room temperature with 50:50 (v/v) acetone:methanol solution (1 mL, maintained at 5 ◦C for 5 min) then washed with PBS (2 × 2 mL) and dried thoroughly in air. One drop of glycerol was added, and covered with a glass slide. A Leica DM3000 microscope was used (Leica Microsystems, Mannheim, Germany) with a Leica Confocal System equipped with a 3 channel multiband scanner Leica TCS SP2. Confocal

fluorescence images were recorded using a 40X Apochromat water-immersion objective lens, with a numerical aperture of 1.4. Ru compounds were imaged using the Ar laser bands at 458, 476 and 488 nm for excitation, and an emission window at 600–700 nm. A 405 nm diode was used to excite DAPI, whose fluorescence was recorded at 450–500 nm. Scanning resolution was set to 1024 × 1024 pixels. Multifocal images of spheroids were acquired with 3 μm intervals between adjacent optical sections, for a total depth of 100 μm. To determine fluorescence related to Ru compounds, 20 different cell areas (60 μm^2) were selected and analyzed for their average fluorescence intensity in the 600–700 nm range, together with a background area (1500 μm^2). Photobleaching was tested on HT-29 cells, selecting an area of 800 μm^2 and irradiating with argon ion laser, at 458 nm, 476 nm or 488 nm, with 5 s impulses for 20 min. A similar but non-irradiated area was used as control. The fluorescence emitted by the cells was recorded as image sequences (1024 × 1024 pixels, 96 dpi and 8 bit colour depth) and fluorescence intensity analysis was performed with the Leica LCS software.

3. Results and discussion

In previous work, the squalenoylation platform developed by our group was employed to design self-assembling nanomedicines derived from hydrophilic therapeutic agents, namely Gem, 2 ,3 -dideoxycytidine, and 2 ,3 -dideoxyinosine (Bekkara-Aounallah et al., 2008; Couvreur et al., 2006). The technology was then extended to include a highly lipophilic drug, PTX (Dosio et al., 2010); it has now been applied to increase the range of applications of in vitro diagnostic tools, resulting in lipophilic prodrugs that produce stable nanosuspensions.

3.1. Synthesis

In order to obtain a compound that is stable in vitro, the luminophor was linked to the squalenoyl moiety via an amide group (Scheme 1). Firstly, an analogue of the complex Ru-BPPBI (Gobetto et al., 2006) (Scheme 1) bearing a linker suitable for conjugation was synthesized. This was achieved by exploiting the reactivity of the ligand's precursor, namely 2-(4-methylpyridin-2- yl)-1H-benzoimidazole, which was regioselectively modified at the NH group by reaction with tert-butyl 6-bromohexylcarbamate. The resulting ligand, tert-butyl 6-(2-(4-methylpyridin-2-yl)- 1H-benzoimidazol-1-yl)-hexylcarbamate, was then reacted with cis-$[Ru(bpy)_2Cl_2]$ to provide the complex [Ru(II) bis(2,2 - bipyridine) {6-[2-(4-methyl-pyridin-2-yl)-1H-benzoimidazol- 1-yl]-hexylamine}]$(PF6)_2$ (Scheme 1A). The new luminophor contains a six-carbon aliphatic chain with a terminal reactive amino group, and was conjugated to the squalenoyl moiety by reaction with an equimolar amount of SQ-NHS in the presence of triethylamine (Scheme 1B), leading to Ru-BPPBI-

hx-SQ in good yield. The advantage of using SQ-NHS, instead of employing an in situ reaction with carbodiimides, lies in the increased yield and reduction of by-products.

3.2. Nanoassemblies: preparation and characterization

The squalenoyl-Ru complex was formulated as nanoassemblies in water, using a simple nanoprecipitation technique without surfactants. Nanoprecipitation of Ru-BPPBI-hx-SQ yielded assemblies of about 300 nm in diameter physically stable, measured via particle size, at concentrations in the range 2–4 mg/mL. In comparison, Ru-BPPBI is poorly soluble in water. The co-nanoassembly of squalenoyl derivatives was achieved by first dissolving both components in acetone and then pouring them both into a rapidly-mixed water solution. Different molar ratios were tested, evaluating the size of the resulting NAs and their stability over time. It was found (Table 1) that, with PTX, which is more hydrophobic and has a more rigid structure, 1:20 is the best Ru-SQ:PTX-SQ ratio; on increasing this ratio, micrometer precipitation rapidly occurred. Conversely, with Gem-SQ, more hydrophilic and more stable, the ratio could be doubled. Fig. 1 shows the opaque and colored appearance of the NAs. For comparison, when equal amounts of two preformed NA solutions were combined, size and charge of PTX-SQ and of Gem-SQ remained substantially unchanged (data not shown). When the quantity of Ru-BPPBI-hx-SQ added to the other prodrug NAs was increased, there first occurred a reduction of mean NA size, and then, at a ratio of 1:1, rapid and complete precipitation. All NAs had negative zeta potential, although Ru-BPPBI-hx-SQ presented the highest value (due to a mixing effect of the complex positive charge, the role of bulky counter-ions, and the solvent) (Cheng, 2006). The physical stability of the NAs was assessed by measuring the size after 15 days' storage at 5 °C. The samples containing Ru-BPPBI-hx-SQ showed a significant size increase, unlike pure PTX and Gem conjugates. Of the co-nanoassemblies, Gem-SQ appeared to improve NA stability.

3.3. Photophysical properties of complexes

Electronic absorption spectra of Ru-BPPBI-hx-SQ and [Ru(II) bis(2,2 -bipyridine) {6-[2-(4-methyl-pyridin-2-yl)-1Hbenzoimidazol-1-yl]-hexylamine}]$(PF6)_2$, recorded at room temperature in acetonitrile solution, were virtually identical to the spectrum of the precursor Ru-BPPBI (Fig. 2). The absorption spectra of the three complexes are characterized by an absorption band centred at 460 nm (ε = 12.2 × 103 L mol−1 cm−1), which is assigned to a metal-to-ligand charge transfer (MLCT) transition. The modification is relatively distant from the metal center, and has little influence on electronic properties. As occurs with the parent complex (Ru-BPPBI), the two derivatives show an intense emission centred at 634 nm, with a quantum yield of 0.02. The

luminescence lies in the red part of the spectrum, distant from any possible autofluorescence of biological material. The luminescence lifetimes of the three complexes are virtually identical: 520 ns for Ru-BPPBI-hx-SQ, and 510 ns for the other two complexes (degassed acetonitrile solution). This long-lived luminescence may be appropriate to explore some of the longer-lasting biodynamic processes (e.g. membrane diffusion, protein rotation, protein folding). Furthermore, the luminescence lifetime of the three complexes is oxygen-sensitive: in air-saturated acetonitrile solution it decreased to 130 ns. When excited at 460 nm, the Ru-BPPBI-hx-SQ Na showed an unstructured emission centered at 630 nm, very similar to the emission of free Ru in acetonitrile solution. Due to the high concentration of luminophor in the NA solution, it was not possible to acquire the absorption spectrum. However, the excitation spectrum recorded at 630 nm is almost identical to the absorption spectrum of free Ru-BPPBI-hx-SQ (Fig. 2). The main difference between NA and free Ru-BPPBI-hx-SQ lies in their luminescence lifetimes. The emission of NA in degassed aqueous solution has a lifetime of 310 ns, shorter than the lifetime of free Ru-BPPBI-hxSQ (510 ns in degassed acetonitrile solution). Conversely, the NA solution is less sensitive to the concentration of dissolved oxygen, and the lifetime decreases only slightly in air-saturated aqueous solution (280 ns).

3.4. In vitro activity: cellular uptake

To investigate cellular uptake and the cytotoxicity of Ru-BPPBIhx-SQ, two well-known human cancer cell lines were used, HT-29 colorectal and MCF-7 breast lines, frequently employed to screen drug compounds and, in particular used to test several Ru complexes (Oehninger et al., 2011; Reddy et al., 2012; Schatzschneider et al., 2008). The cellular localization of the complexes was studied by CLSM, and Figs. 3 and 4 show characteristic cellular staining patterns. DAPI, a fluorescent stain for DNA, was used to stain the cell nucleus clearly. In a typical protocol, Ru-BPPBI-hx-SQ NA and the parent compound were diluted to a final concentration of 50 μM and incubated for 2 h. The CLSM experimental conditions were set to 458–488 nm for the range for excitation, corresponding to MLCT transition, while the absorbance of the metal complex and the emission images were recorded at 600–620 nm. No DAPI interference with Ru complex luminescence occurred (Abs max 358 nm, emission maximum 461 nm). Very little luminescence was observed inside HT-29 cells treated with Ru-BPPBI (Fig. 3, top) indicating that the dye cannot easily penetrate the cell membrane and enter the cell, even after 2 h incubation. This confirmed data reported for [Ru(bpy)2-(4- carboxyphenyl)imidazo[4,5-f] (phen)]$^{2+}$ (Neugebauer et al., 2008) and for [Ru(bpy)^{2}dppz]$^{2+}$ and [Ru(phen)^{2}dppz]$^{2+}$ (Puckett and Barton, 2007) (phen = 1,l0-phenanthroline; dppz = dipyrido[3,2- a:2 ,3 -c]phenazine). In contrast (Fig. 3, bottom), Ru-BPPBI-

hx-SQ is passively transported through the cell membrane and accumulates inside the cell: the luminescence intensity of the cell population increased by 400%. Interestingly, the cell nucleus was equally stained, unlike what has been reported in other studies (Puckett and Barton, 2007) for a highly hydrophobic $Ru(DIP)_2dppz^{2+}$ (DIP = 4,7-diphenyl-1,10-phenanthroline) derivative. Fig. 4 shows the luminescence emitted by MCF-7 when stained with Ru-BPPBIhx-SQ: ruthenium luminescence is clearly visible throughout the cytoplasm. Inductively-coupled plasma mass spectrometry (ICP-MS) measurements were performed to quantify the amount of Ru taken up by cells. MCF-7 cells were treated with 50 M of Ru-BPPBI or Ru-BPPBI-hx-SQ in serum-free medium. ICP-MS measures gave 270 ± 12 amol of Ru per cellfor Ru-BPPBI-hx-SQ and 13± 6 amol per cell for the non-squalenoyl complex. These results confirmed the distribution of the lipophilic complex inside the cell, and indicated Fthat the concentration of the squalenoyl complex (160 M) within the cell was substantial, well above the exposure concentration. To improve our knowledge of cell uptake and diffusion of squalenoyl derivatives, experiments were also run on threedimensional cell cultures. This method has the advantage of maintaining some of the in vivo cellular architecture and interactions of cancer cells. Furthermore, the spheroids are a model of micrometastatic, prevascularized tumors (Helmlinger et al., 1997; Jacks and Weinberg, 2002). Fig. 5 is a representative CLSM equatorial section image of an HT-29 spheroid incubated for 2 h with Ru-BPPBI-hx-SQ. The luminescence is widely diffused and only the inner core appears dark. These results clearly demonstrate that the high lipophilicity of the compound allows it to bind to the spheroid rim, and provides rapid diffusion among intracellular spaces, leading to well-distributed intratumoral penetration.

3.4.1. Cytotoxicity

In order to evaluate the role of Ru-complexes on cell viability, HT-29 and MCF-7 cell lines were incubated extensively (72 h at 37 ◦C, 5% CO2 in media with foetal calf serum) with high concentrations (up to 2 mM) of compound. Inhibition of protein synthesis was checked by measuring the incorporation of tritiated leucine. Ru-BPPBI presented an IC50 of 270 and 420 μM, on MCF7 and HT- 29 cells respectively. The squalenoyl derivative appeared as toxic as the parent compound against HT-29 cells (IC50 380 μM) and slightly more toxic against MCF-7 (110 μM). It is important for a cell-imaging probe to have very low cytotoxicity, and squalenoylation, applied to potent anticancer agents, has been found to modulate their cytoxicity, reducing systemic side effects (Dosio et al., 2010; Raouane et al., 2011; Réjiba et al., 2011). In the present case, although a significant increase in lipophilicity was observed, with a related increase in cellular diffusion, the Ru complex did not cause significant inhibition of protein synthesis. It is important to note that, in

the case of other Ru(II) compounds, for example [Ru (bpy)2(N-N)]$^{2+}$ containing lipophilic bidentate aromatic ligands, the toxicity rose to 3 μM (against MCF-7) and to 6 μM (against HT-29) when tested with the same incubation times used Fig. 6. Trend of Ru-BPPBI-hx-SQ luminescence emission after 20 min of continuous irradiation of treated HT-29 cells used here (Schatzschneider et al., 2008). This toxicity level of the ruthenium(II) polypyridyl complexes is similar to that of cisplatin, a potent anticancer agent.

3.4.2. CLSM to monitor photobleaching of the Ru complex

A drawback of conventional organic chromophores for laser scanning microscopy is their propensity to photobleach, which limits their use over extended periods (Diaspro et al., 2006). Under the imaging conditions given above, selected area containing a group of HT-29 cells, previously incubated with Ru-BPPBI-hx-SQ, were submitted to 20 min of continuous pulsed irradiation. The diffused compound retained more than 60% of its initial luminescence intensity (Fig. 6). This photostability, combined with uniform diffusion inside cells, may make the complex useful for studying the dynamics of cellular processes.

4. Conclusions

This study reports the production of a Ru complex capable of self-assembling into nanoparticles in aqueous media. Even for the bulky aromatic Ru complex (volume of 4005.9 Å^3) (Gobetto et al., 2006), the bioconjugate obtained by linking the squalenoyl moiety provided a supramolecular assembly, as occurs with other planar metal complexes such as cis-platin (Arias et al., 2011). The lipophilicity induced by the squalene chain appeared to be flexible, and to improve cell uptake and diffusion, including in multicellular spheroids. It also packed, to allow supramolecular assembly as occurs with other drug squalenoyl derivatives. Unlike Gem-SQ, which is metabolized by the endothelial reticulum and does not penetrate the cell nucleus (Bildstein et al., 2010), Ru-BPPBI-hxSQ concentrates inside the cell, diffusing into the cytoplasm and intracellular organs. It is also able to diffuse throughout a more organized cell system, in the form of multicellular spheroid. Further, unlike other bidentate aromatic derivatives (Schatzschneider et al., 2008), Ru-BPPBI-hx-SQ does not exercise significant toxicity. Preliminary studies of the co-nanoassembly show that this Ru-complex may be distributed inside drug-SQ prodrugs, and appears to stabilize the Gem-SQ NA to a greater extent than does PTX-SQ. Further studies will be required to fully determine the structure of co-nanoassemblies. Moreover, other in vitro studies are needed to evaluate the role of the individual components of co-nanoassemblies in the release, uptake and diffusion into cells.

However, the squalenoylation platform has demonstrated its relevance, not only in the drugability of therapeutic agents, but also for the development of novel cell diagnostic tools.

Acknowledgments

Confocal images were acquired at the Laboratorio di Microscopie Avanzate of the University of Turin, and we thank Dr Andrea Genre for useful discussions and assistance during studies. The authors affiliated to the Dipartimento di Scienza e Tecnologia del Farmaco at Turin University warmly thank the Consortium TEFARCO Innova for research support.

References

Arias, J.L., Reddy, L.H., Othman, M., Gillet, B., Desmaele, D., Zouhiri, F., Dosio, F., Gref, R., Couvreur, P., 2011. Squalene based nanocomposites: a new platform for the design of multifunctional pharmaceutical theragnostics. ACS Nano 5, 1513–1521.

Barni, E., Savarino, P., 1977. 2-(Methylpyridyl or quinolyl)benz-X-azoles. J. Heterocyclic Chem. 14, 937–940.

Bekkara-Aounallah, F., Gref, R., Othman, M., Reddy, L.H., Pili, B., Allain, V., Bourgaux, C.,Hillaireau,H., Lepetre-Mouelhi, S., Desmaele, D., Nicolas,J.,Chafi, N.,Couvreur, P., 2008. Novel PEGylated nanoassemblies made of self-assembled squalenoyl nucleoside analogues. Adv. Funct. Mater. 18, 3715–3725.

Besic Gyenge, E., Darphin, X., Wirth, A., Pieles, U., Walt, H., Bredell, M., Maake, C., 2011. Uptake and fate of surface modified silica nanoparticles in head and neck squamous cell carcinoma. J. Nanobiotechnol., 9.

Bildstein, L., Dubernet, C., Marsaud, V., Chacun, H., Nicolas, V., Gueutin, C., Sarasin, A., Bonech, H., Lepatre-Mouelhi, S., Desmaele, D., Couvreur, P., 2010. Transmembrane diffusion of gemcitabine by a nanoparticulate squalenoyl prodrug: an original drug delivery pathway. J. Control. Release 147, 163–170.

Boerner, L.J.K., Zaleski, J.M., 2005. Metal complex–DNA interactions: from transcription inhibition to photoactivated cleavage. Curr. Opin. Chem. Biol. 9, 135–144.

Ceruti, M., Balliano, G., Viola, F., 1987. Synthesis and biological activity of azasqualenes, bis-azasqualenes and derivatives. Eur. J. Med. Chem. 22, 199–208. Cheng, K.L., 2006. The negative charge of nanoparticles. Microchem. J. 82, 119–120.

Couvreur, P., Stella, B., Reddy, L.H., Hillaireau, H., Dubernet, C., Desmaele, D., LepetreMouelhi, S., Rocco, F., Dereuddre-Bosquet, N., Clayette, P., Rosilio, V., Marsaud, V., Renoir, J.-M., Cattel, L., 2006. Squalenoyl nanomedicines as potential therapeutics. Nano Lett. 6, 2544–2548.

Diaspro, A., Chirico, G., Usai, C., Ramoino, P., Dobrouki, J., 2006. Photobleaching. In: Pawley, J. (Ed.), Handbook of Biological Confocal Microscopy. Springer, New York, pp. 690–702.

Dosio, F., Reddy, L.H., Ferrero, A., Stella, B., Cattel, L., Couvreur, P., 2010. Novel nanoassemblies composedof squalenoyl-paclitaxelderivatives: Synthesis, characterization, and biological evaluation. Bioconjugate Chem. 21, 1349–1361.

Elmes, R.B.P., Orange, K.N., Cloonan, S.M., Williams, D.C., Gunnlaugsson, T., 2011. Luminescent ruthenium(II) polypyridyl functionalized gold nanoparticles, their DNA binding abilities and application as cellular imaging agents. J. Am. Chem. Soc. 133, 15862–15865.

Fernandez-Moreira, V., Thorp-Greenwood, F.L., Coogan, M.P., 2010. Application of d6 transition metal complexes in fluorescence cell imaging. Chem. Commun. 46, 186–202.

Gerritsen, H.C., Sanders, R., Draaijer, A., Ince, C., Levine, Y.K., 1997. Fluorescence lifetime imaging of oxygen in living cells. J. Fluoresc. 7, 11–15.

Gobetto, R., Caputo, G., Garino, C., Ghiani, S., Nervi, C., Salassa, L., Rosenberg, E., Ross, J.B.A., Viscardi, G., Martra, G., Miletto, I., Milanesio, M., 2006. Synthesis, electrochemical and electrogenerated chemiluminescence studies of ruthenium(II) bis(2,2 -bipyridyl){2-(4-methylpyridin-2-yl)benzo[d]-X- azole} complexes. Eur. J. Inorg. Chem., 2839–2849.

Hart, J.R., Glebov, O., Ernst, R.J., Kirsch, I.R., Barton, J.K., 2006. DNA mismatchspecific targeting and hypersensitivity of mismatch-repair-deficient cells to bulky rhodium(III) intercalators. Proc. Natl. Acad. Sci. U.S.A. 103, 15359–15363.

Helmlinger, G., Netti, P.A., Lichtenbeld, H.C., Melder, R.J., Jain, R.K., 1997. Solid stress inhibits the growth of multicellular tumor spheroids. Nat. Biotechnol. 15, 778–783.

Jacks, T., Weinberg, R.A., 2002. Taking the study of cancer cell survival to a new dimension. Cell 111, 923–925.

Juris, A., Balzani, V., Barigelletti, F., Campagna, S., Belser, P., Vonzelewsky, A., 1988. Ru(II) polypyridine complexes—photophysics, photochemistry, electrochemistry, and chemi-luminescence. Coord. Chem. Rev. 84, 85–277.

Le Gac, S., Rickling, S., Gerbaux, P., Defrancq, E., Moucheron, C., Kirsch-De Mesmaeker, A., 2009. A photoreactive ruthenium(II) complex tethered to a guanine-containing oligonucleotide: A biomolecular tool that behaves as a seppuku molecule. Angew. Chem. Int. Ed. 48, 1122–1125.

Lentz, F., Drescher, A., Lindauer, A., Henke, M., Hilger, R.A., Hartinger, C.G., Scheulen, M.E., Dittrich, C., Keppler, B.K., Jaehde, U., 2009. Pharmacokinetics of a novel anticancer ruthenium complex (KP1019, FFC14A) in a phase I dose-escalation study. Anticancer Drugs 20, 97–103.

Levina, A., Mitra, A., Lay, P.A., 2009. Recent developments in ruthenium anticancer drugs. Metallomics 1, 458–470.

Lo, K.K.-W., Lee, T.K.-M., Lau, J.S.-Y., Poon, W.-L., Cheng, S.-H., 2008. Luminescent biological probes derived from ruthenium(II) estradiol polypyridine complexes. Inorg. Chem. 47, 200–208.

Lo, K.K.W., Lee, T.K.M., 2007. Luminescent ruthenium(II) amidodipyridoquinoxaline biotin complexes that display higher avidin-induced emission enhancement. Inorg. Chim. Acta 360, 293–302.

Neugebauer, U., Pellegrin, Y., Devocelle, M., Forster, R.J., Signac, W., Morand, N., Keyes, T.E., 2008. Ruthenium polypyridyl peptide conjugates: membrane permeable probes for cellular imaging. Chem. Commun., 5307–5309.

Oehninger, L., Alborzinia, H., Ludewig, S., Baumann, K., Wölfl, S., Ott, I., 2011. From catalysts to bioactive organometallics: do Grubbs catalysts trigger biological effects? ChemMedChem 6, 2142–2145.

Ogura, H., Nagai, S., Takeda, K., 1980. A novel reagent(N succinimidyl diphenylphosphate)for synthesis of active ester andpeptide. TetrahedronLett. 21, 1467–1468.

Puckett, C.A., Barton, J.K., 2007. Methods to explore cellular uptake of ruthenium complexes. J. Am. Chem. Soc. 129, 46–47.

Raouane, M., Desmaele, D., Gilbert-Sirieix, M., Gueutin, C., Zouhiri, F., Bourgaux, C., Lepeltier, E., Gref, R., Ben Salah, R., Clayman, G., Massaad-Massade, L., Couvreur, P., 2011. Synthesis, characterization, and in vivo delivery of siRNA-squalene nanoparticles targeting fusion oncogene in papillary thyroid carcinoma. J. Med. Chem. 54, 4067–4076.

Reddy, V.D., Dayal, D., Szalda, D.J., Cosenza, S.C., Ramana Reddy, M.V., 2012. Syntheses, structures, and anticancer activity of novel organometallic ruthenium–maltol complexes. J. Organomet. Chem. 700, 180–187.

Réjiba, S., Reddy, L.H., Bigand, C., Parmentier, C., Couvreur, P., Hajri, A., 2011. Squalenoyl gemcitabine nanomedicine overcomes the low efficacy of gemcitabine therapy in pancreatic cancer. Nanomed. Nanotechnol. 7, 841–849.

Schatzschneider, U., Niesel, J., Ott, I., Gust, R., Alborzinia, H., Wölfl, S., 2008. Cellular uptake, cytotoxicity, and metabolic profiling of human cancer cells treated with ruthenium(II) polypyridyl complexes [Ru(bpy)2(N-N)]Cl2 with N-N=bpy, phen, dpq, dppz, and dppn. ChemMedChem 3, 1104–1109.

Schroeder, A., Heller, D.A.,Winslow, M.M., Dahlman, J.E., Pratt, G.W., Langer, R., Jacks, T., Anderson, D.G., 2012. Treating metastatic cancer with nanotechnology. Nat. Rev. Cancer 12, 39–50.

Scolaro, C., Bergamo, A., Brescacin, L., Delfino, R., Cocchietto, M., Laurenczy, G., Geldbach, T.J., Sava, G., Dyson, P.J., 2005. In vitro and in vivo evaluation of ruthenium(II)–arene PTA complexes. J. Med. Chem. 48, 4161–4171.

Sullivan, B.P., Salmon, D.J., Meyer, T.J., 1978. Mixed phosphine 2,2 -bipyridine complexes of ruthenium. Inorg. Chem. 17, 3334–3341.

Wartenberg, M., Acker, H., 1995. Quantitative recording of vitality patterns in living multicellular spheroids by confocal microscopy. Micron 26, 395–404.

Zeglis, B.M., Barton, J.K., 2008. Binding of Ru(bpy)2(eilatin)2+ to matched and mismatched DNA. Inorg. Chem. 47, 6452–6457.

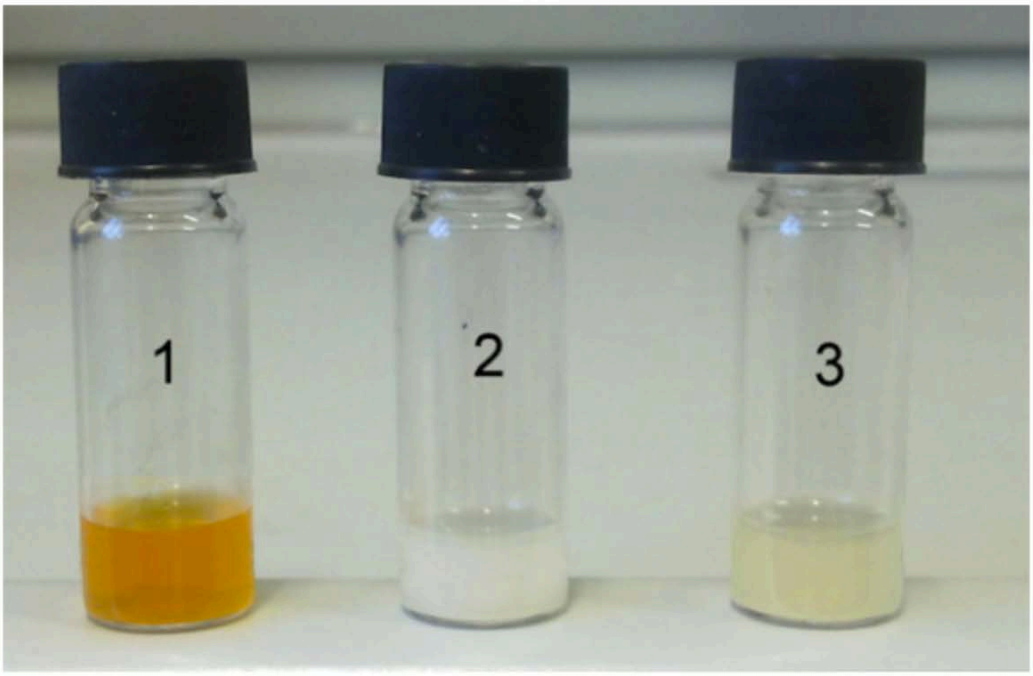

Fig. 1. Nanoassemblies of Ru-BPPBI-hx-SQ (1) and co-nanoassemblies of PTX-SQ (2) with a 1:20 molar ratio of Ru-BPPBI-hx-SQ, and Gem-SQ with a 1:10 molar ratio of Ru-BPPBI-hx-SQ (3).

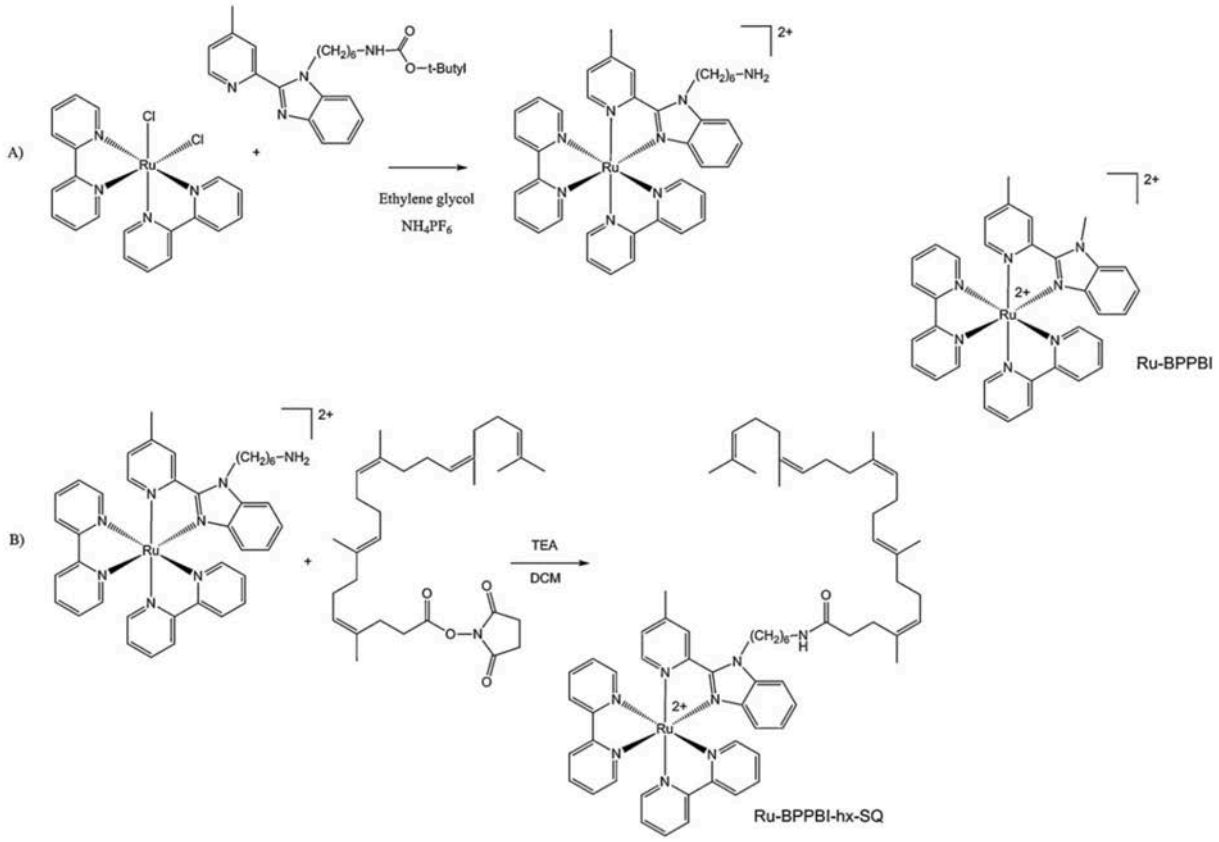

Scheme 1. Synthesis of the compound [Ru(II) bis(2,2′-bipyridine) {6-[2-(4-methyl-pyridin-2-yl)-1*H*-benzoimidazol-1-yl]-hexylamine}]$(PF_6)_2$ (A), Ru-BPPBI-hx-SQ (B) and structure of Ru-BPPBI.

Table 1
Physicochemical characterization and stability of the squalenoyl Ru compound and co-nanoassemblies.

Compound/NA	Mean particle size (nm ± S.D.)	Polydispersity index	Zeta potential (mV ± S.D.)	NA stability (size, nm) 15 days, 5 °C
Ru-DPPBI-SQ	307 ± 22.2	0.215	−7.25 ± 1.6	540 ± 26.3
PTX-SQ	120 ± 8.2	0.085	−36.91 ± 8.3	130 ± 4.2
Gem-SQ	135 ± 10.2	0.125	−28.12 ± 5.6	142 ± 7.3
PTX-SQ+ Ru-BPPBI-hx-SQ[a]	162 ± 5.7	0.191	−22.12 ± 9.6	310 ± 6.2
Gem-SQ+ Ru-BPPBI-hx-SQ[b]	226 ± 6.8	0.229	−12.32 ± 2.5	285 ± 8.6

[a] Molar ratio of the NA composition PTX-SQ:Ru-SQ 20:1.
[b] Molar ratio of the NA composition Gem-SQ:Ru-SQ 10:1.

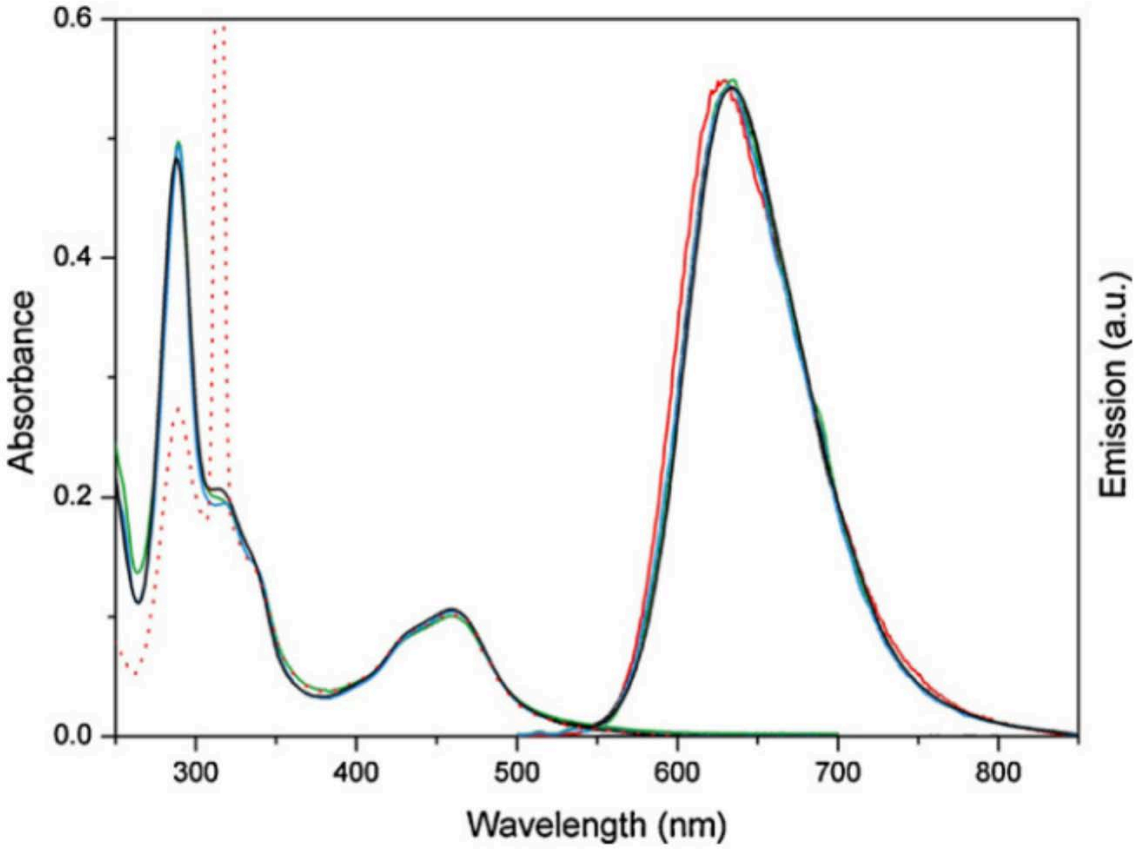

Fig. 2. Absorption (left) and emission (right) spectra of Ru-DPPBI (black), Ru-BPPBI-hx-SQ (green), Ru-BPPBI-hx-SQ nanoassembly (red) and [Ru(II) bis(2,2′-bipyridine) {6-[2-(4-methyl-pyridin-2-yl)-1H-benzoimidazol-1-yl]-hexylamine}$(PF_6)_2$. (For interpretation of the references to color in figure legend, the reader is referred to the web version of the article.)

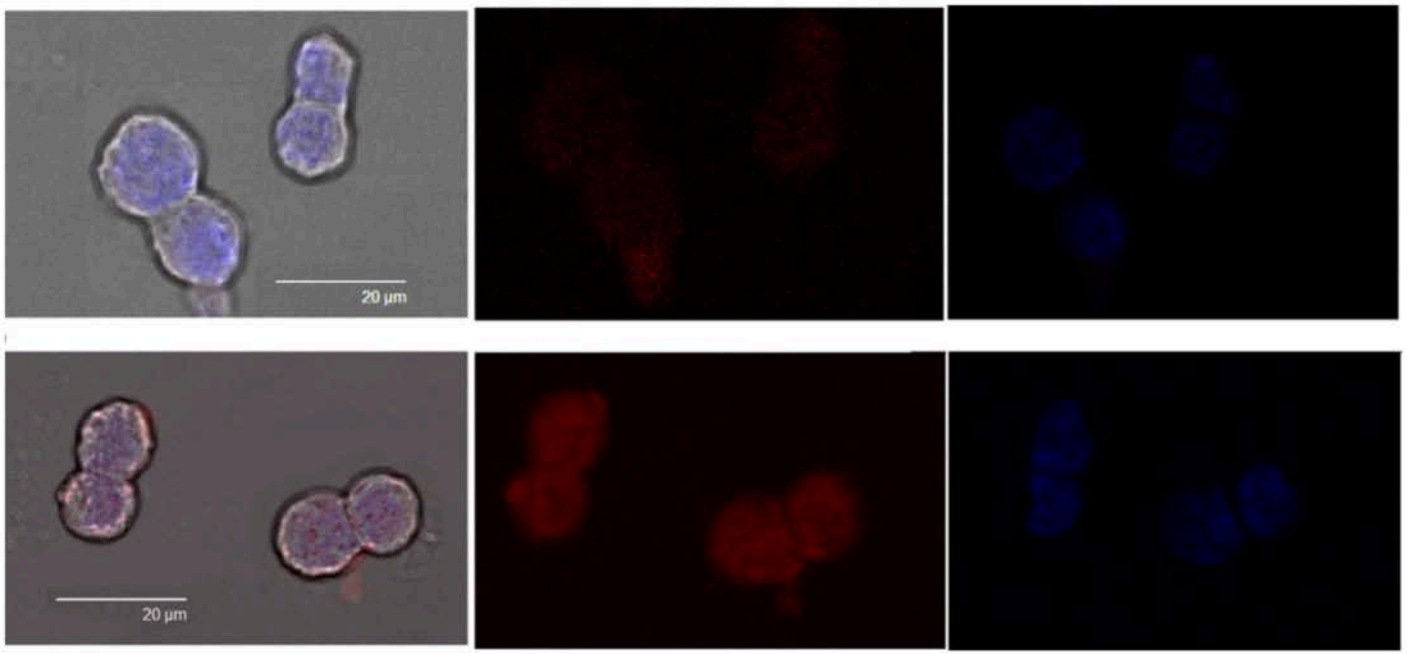

Fig. 3. Confocal microscopy of HT-29 cells treated with Ru-BPPBI (top) or Ru-BPPBI-hx-SQ NA (bottom) at 50 µM for 2 h at 37 °C. From left to right, images are taken as merged (white light + red + blue), emission due to Ru complex, and emission due to DAPI. (For interpretation of the references to color in figure legend, the reader is referred to the web version of the article.)

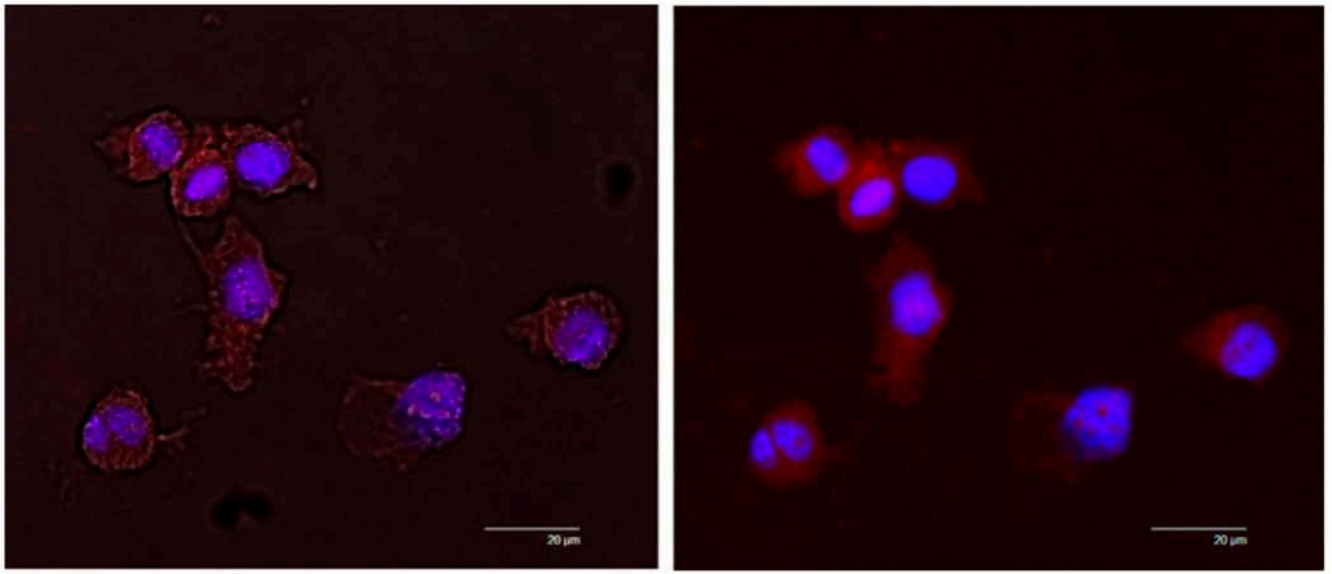

Fig. 4. Confocal microscopy of MCF-7 cells treated with Ru-BPPBI-hx-SQ NA at 50 µM for 2 h at 37 °C. From left to right, images are taken as merged (white light + red + blue), and emission due to Ru complex plus DAPI. (For interpretation of the references to color in figure legend, the reader is referred to the web version of the article.)

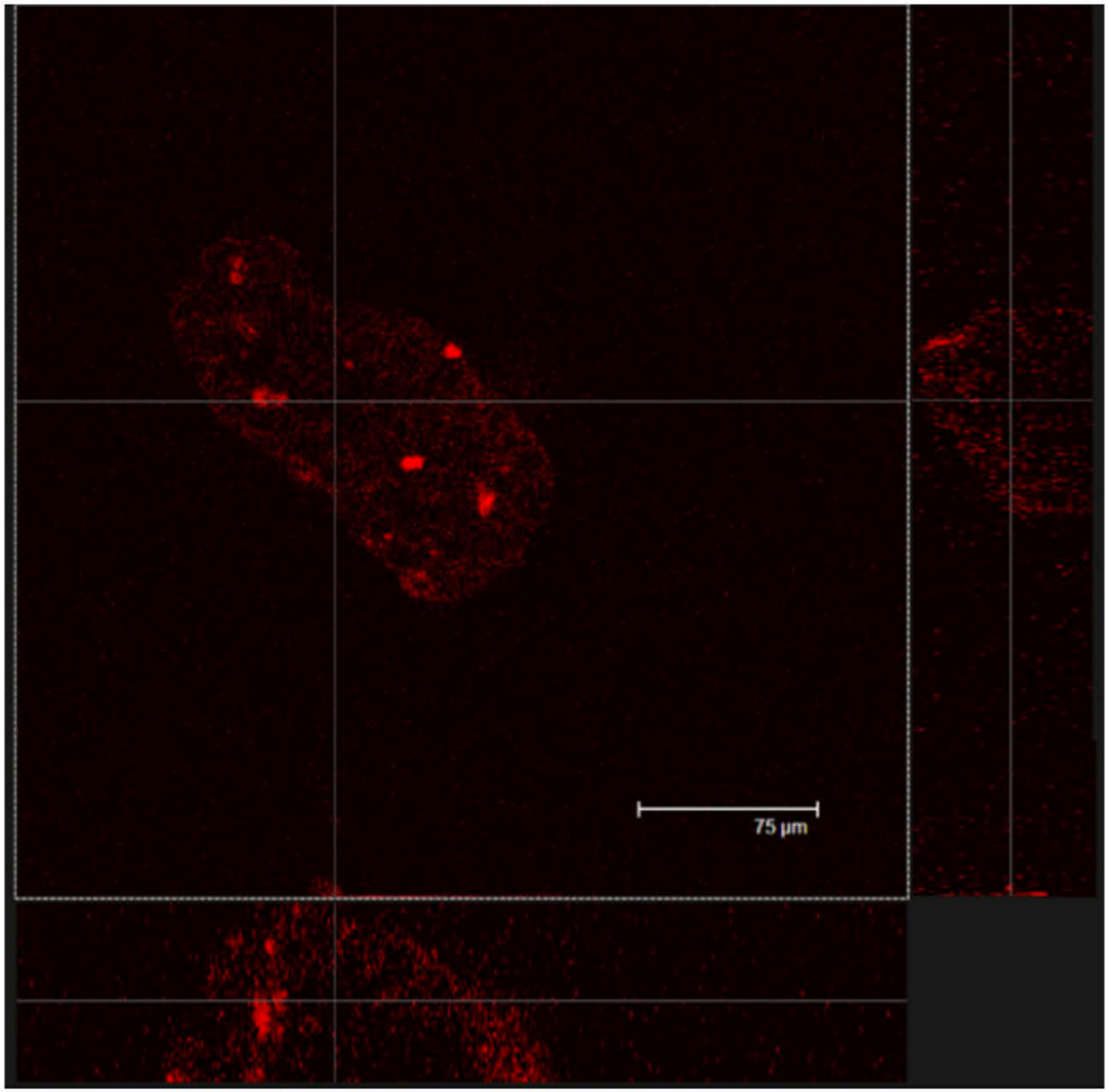

Fig. 5. Orthogonal views, obtained in an equatorial optical level, of whole HT-29 spheroids treated with Ru-BPPBI-hx-SQ NAs at 50 µM for 2 h at 37 °C. Images show the diffusion of fluorescence both in the surface layer and up to half thickness of the spheroid (right and bottom panels).

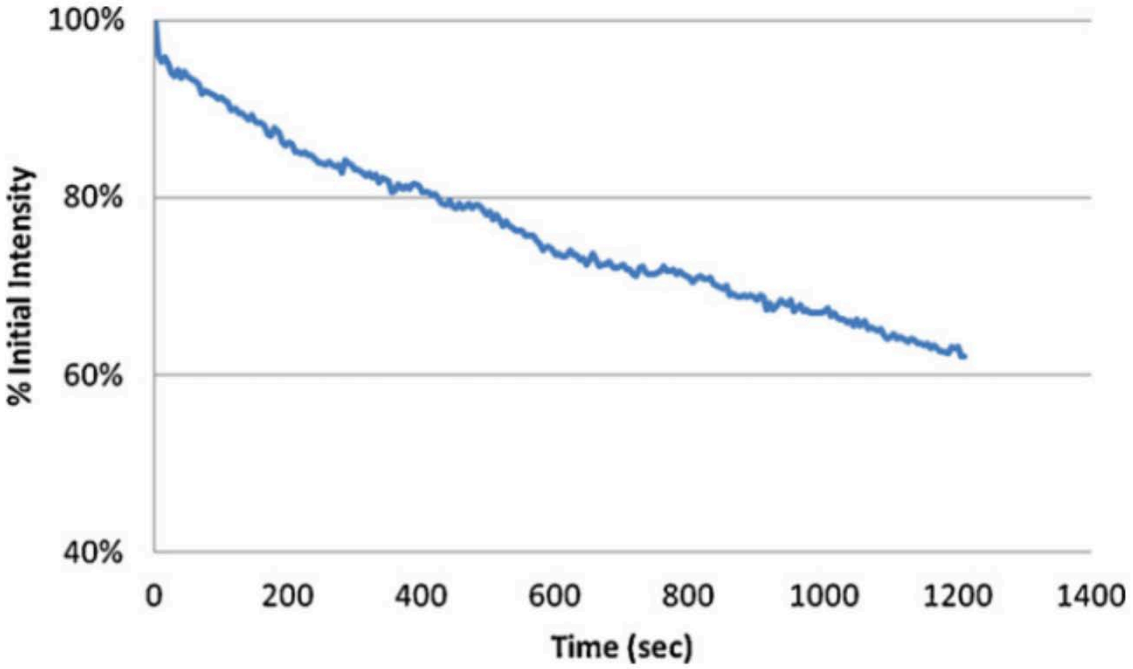

Fig. 6. Trend of Ru-BPPBI-hx-SQ luminescence emission after 20 min of continuous irradiation of treated HT-29 cells.